Journal of Power Sources 190 (2009) 346–350

Contents lists available at ScienceDirect

Journal of Power Sources

journal homepage: www.elsevier.com/locate/jpowsour

Short communication

An alkaline direct $NaBH_4$–H_2O_2 fuel cell with high power density

Dianxue Cao*, Dandan Chen, Jian Lan, Guiling Wang

College of Material Science and Chemical Engineering, Harbin Engineering University, Harbin 150001, PR China

ARTICLE INFO

Article history:
Received 3 December 2008
Received in revised form
25 December 2008
Accepted 30 December 2008
Available online 14 January 2009

Keywords:
Pt–Ru
Pd–Ir
Borohydride, hydrogen peroxide
Liquid alkaline fuel cell

ABSTRACT

A high performance alkaline direct borohydride–hydrogen peroxide fuel cell with Pt–Ru catalyzed nickel foam as anode and Pd–Ir catalyzed nickel foam as cathode is reported. The electrodes were prepared by electrodeposition of the catalyst components on nickel foam. Their morphology and composition were analyzed by SEM–EDX. The effects of concentrations of $NaBH_4$ and H_2O_2 as well as operation temperature on the cell performance were investigated. The cell exhibited an open circuit voltage of about 1.0 V and a peak power density of 198 mW cm^{-2} at a current density of 397 mA cm^{-2} and a cell voltage of 0.5 V using 0.2 mol dm^{-3} $NaBH_4$ as fuel and 0.4 mol dm^{-3} H_2O_2 as oxidant operating at room temperature. Electrooxidation of $NaBH_4$ on Pt–Ru nanoparticles was studied using a rotating disk electrode and complete $8e^-$ oxidation was observed in 2 mol dm^{-3} NaOH solution containing 0.01 mol dm^{-3} $NaBH_4$.

1. Introduction

As promising power sources for space and underwater applications, direct borohydride–hydrogen peroxide fuel cells (DBHPFCs), comprised of BH_4^- oxidation at the anode and H_2O_2 reduction at the cathode, have attracted increasing attentions recently [1–6]. The main issues for DBHPFC encountered concern the hydrolysis and incomplete electrooxidation of BH_4^- at the anode resulting in evolution of H_2 [7] and the chemical decomposition of H_2O_2 at the cathode leading to the formation of O_2 [5]. The generation of H_2 and O_2 not only reduce the energy density of DBHPFC, but also cause problems in the design and safety managements of the cells. Therefore, most researches on DBHPFC focus on developments of anode and cathode electrocatalysts having a low catalytic activity for BH_4^- hydrolysis [8–15] and H_2O_2 decomposition [4,5,16]. The types of anode catalysts examined include noble metals (Pd, Pt, Au, Os, Ag), transition metals (Ni, Cu), and hydrogen storage alloys (AB_5- and AB_2-type). However, only Au shows promising results. It can catalyze the complete $8e^-$ oxidation of BH_4^- [12,14,15,17], but has relatively low activity. Au can also minimize H_2O_2 decomposition while providing reasonable activity for electroreduction of H_2O_2 [5].

Current DBHPFC generally adopt the membrane electrode assembly (MEA) as their core component and operate on relatively high concentration BH_4^- and H_2O_2 to achieve high power output. However, high concentrations of BH_4^- and H_2O_2 favor evolution of H_2 at the anode and O_2 at the cathode, which cause a two-phase counter current flow in the electrode layers, and adversely affect reactant diffusions [18]. Therefore, DBHPFC with MEA require a highly selective electrocatalyst, such as Au, which is however not sufficiently active for achieving high power output. In this study, novel electrodes having a three-dimensional network structure with micro-open cages were investigated. This type of electrode shows excellent diffusion properties and is particularly suitable for liquid–liquid fuel cells with gas products, like DBHPFC. Besides, it allows the use of low concentration reactants, which limits gas byproduct generation. Pt–Ru was used as the anode catalyst. The idea is using Ru to catalyze complete hydrolytic decomposition of BH_4^- generating adsorbed hydrogen, and using Pt to catalyze the electrooxidation of resulting hydrogen to realize *in situ* indirect complete oxidation of BH_4^-. It has been reported that Pt–Ru shows high catalytic activity for BH_4^- electrooxidation, and Pt–Ru is a bifunctional catalyst with Ru serving mainly as the hydrolysis catalyst of BH_4^- and Pt acting as the electrocatalyst for both H_2 and BH_4^- oxidation [7]. Pd–Ir was used as the cathode catalyst taking advantage of its high activity for H_2O_2 electroreduction [4]. The combination of highly active electrocatalysts and the novel electrode structure enables DBHPFC to achieve high power output with depressed H_2 and O_2 evolution.

2. Experimental

Electrochemical measurements were performed in a standard three-electrode electrochemical cell using a computerized potentiostat (Autolab PGSTAT302, Eco Chemie) controlled by GPES software. A glassy carbon rod behind a D-porosity glass frit was employed as the counter electrode and a saturated Ag/AgCl, KCl

* Corresponding author. Tel.: +86 451 82589036; fax: +86 451 82589036.
E-mail address: caodianxue@hrbeu.edu.cn (D. Cao).

0378-7753/$ – see front matter © 2009 Elsevier B.V. All rights reserved.
doi:10.1016/j.jpowsour.2008.12.134

electrode served as the reference. All potentials were referred to the reference electrode. Commercial Pt–Ru black (HiSPEC™6000, Pt:Ru = 1:1 atomic ratio, Alfa Aesar) was used for the rotating disk electrode (RDE) investigation. A suspension of 2.5 mg cm^{-3} Pt–Ru in water was prepared by sonication for 30 min. 4.2×10^{-3} cm^{-3} (10.5 μg) of the catalyst suspension was placed onto a glassy carbon RDE (d = 3 mm, Autolab) and dried in air at room temperature for 2 h. A thin layer of Pt–Ru nanoparticles was thus formed on the RDE surface, yielding a catalyst loading of approximately 150 μg cm^{-2}. RDE voltammograms were obtained consecutively from low to high rotation rate after the curve at the lowest ration rate (625 rpm) stabilized.

The anode and cathode for DBHPFC tests were prepared by electrochemical co-deposition of Pt–Ru and Pd–Ir on Ni foam (110 PPI, 320 g m^{-2}, ShunDe Canafull industry Co. Ltd., China), respectively. The dimension of the Ni foam support is 22.4 mm × 22.4 mm × 1 mm (length × width × thickness), which gives a 5 cm^2 nominal planar area of the electrode. This area is used to calculate current densities of the DBHPFC test cell. Ni foams were degreased with acetone, etched with 6.0 mol dm^{-3} HCl for 15 min, and rinsed with ultrapure water prior to use. Pt–Ru deposition was carried as follows: Ni foam electrode was immersed in an electrolyte solution consisting of 20 mmol dm^{-3} H_2PtCl_6, 20 mmol dm^{-3} $RuCl_3$ and 0.2 mol dm^{-3} KCl at open circuit potential (OPC) and hold at OPC for 1 min. The shiny grey Ni foam turned to black. The electrode was then cycled between −0.50 and 0.0 V for 10 times at a scan rate of 10 mV s^{-1}, removed from the electrolyte solution, washed with ultrapure water thoroughly, and dried at 60 °C for 20 min under N_2 stream. The above procedure was repeated 4 times to obtain the final Pt–Ru on Ni foam anode. Pd–Ir deposition was performed using a procedure similar with Pt–Ru deposition, except that the electrolyte solution was 10 mmol dm^{-3} $PdCl_2$ + 20 mmol dm^{-3} H_2IrCl_6 + 0.1 mol dm^{-3} HCl + 0.2 mol dm^{-3} KCl, and the potential cycling was carried out between −0.35 and −0.15 V for 20 times at 10 mV s^{-1}. The resulting electrodes were kept in 1 mol dm^{-3} $NaBH_4$ + 2 mol dm^{-3} NaOH before use. All solutions were made with analytical grade chemical reagents and Millipore Milli-Q water (18 MΩ cm). The morphology of the electrodes and the composition of catalysts were examined using scanning electron microscopy (SEM; JEOL JSM-6480) equipped with an energy-dispersive X-ray spectrometer (EDX).

The structure of the DBHPFC test cell is similar to that of conventional direct methanol fuel cells. The sandwich of anode/membrane (Nafion®-115)/cathode was compressed between two graphite block current collectors with a serpentine flow field. Silicon gaskets were assembled in between the electrode and the graphite block to act as spacers. The electrode area is 5 cm^2. Two peristaltic pumps were used to circulate the anolyte and the catholyte both at a 40 cm^3 min^{-1} flow rate. The cell voltage–current curves were recorded using a computer-controlled E-load system (Arbin). The Nafion®-115 membrane was cleaned by boiling in 3% H_2O_2 for 1 h, followed by boiling in ultrapure water for 2 h with the water being changed every 30 min. The cleaned membrane was soaked in 2 mol dm^{-3} NaOH for 1 h prior to use.

3. Results and discussion

3.1. Rotating disk electrode study for BH_4^- electrooxidation on Pt–Ru nanoparticles

Fig. 1 shows polarization curves for $NaBH_4$ reduction in 2 mol dm^{-3} NaOH containing 0.01 mol dm^{-3} $NaBH_4$. The onset potential for BH_4^- oxidation on Pt–Ru is about −1.05 V, which is more negative than that on Au [15], but is close to that on Pt [8]. Currents reach their limits at potentials around −0.9 and −0.8 V. These results demonstrate the high activity of Pt–Ru. The insert of

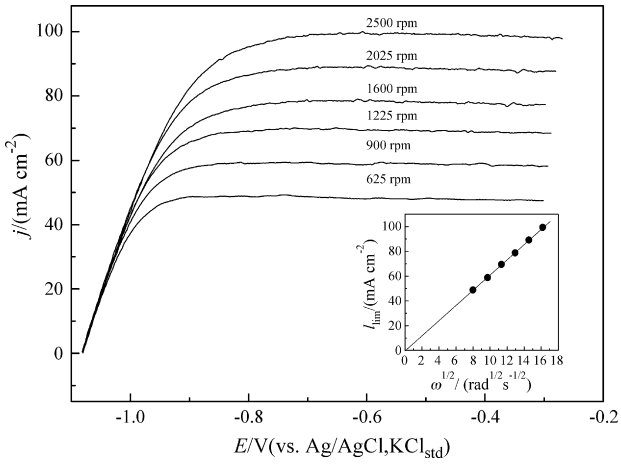

Fig. 1. Linear sweep voltammograms for borohydride oxidation on a Pt–Ru modified Au rotating disk electrode at different rotating rates. Electrolyte: 0.01 mol dm^{-3} $NaBH_4$ in 2 mol dm^{-3} NaOH solution; scan rate: 50 mV s^{-1}; temperature: 25 °C. Insert is the corresponding plot of j_{lim} at 0.6 V vs. $\omega^{1/2}$.

Fig. 1 shows that the plot of limiting current density measured at −0.6 V (j_{lim}) versus $\omega^{1/2}$ is linear with zero intercept, indicating that experimental data is in agreement with Levich's theory. The number of electrons exchanged per BH_4^- was thus determined by the Levich equation (Eq. (1)):

$$j_{lim} = 0.620nFD^{2/3}C^*\nu^{-1/6}\omega^{1/2} \quad (1)$$

where j_{lim} (mA cm^{-2}) is the limiting current density, n the number of electrons transferred for the oxidation of per BH_4^-, F the Faraday constant (96,485 C mol^{-1}), D the BH_4^- diffusion coefficient (1.6×10^{-5} cm^2 s^{-1}) [15], C^* the BH_4^- concentration in the solution (0.01 mol dm^{-3}), ν the NaOH solution kinematic viscosity (1.19×10^{-2} cm^2 s^{-1}) [15] and ω the RDE revolution rate (rad s^{-1}). The apparent number of electrons calculated from the slope of the plot is 7.8, indicating that the oxidation of BH_4^- is nearly complete. We also found that the number of electrons is about 6 for Pt nanoparticles (HiSPEC™1000, Alfa Aesar), and Pt–Ru generates higher current densities than Pt at the potential range from −0.9 to −0.6 V. A total of eight electrons can be generated either by complete direct oxidation of BH_4^- (direct pathway) or by complete hydrolytic decomposition of BH_4^- to H_2 following by oxidation of the resulting H_2 with 100% efficiency (indirect pathway). For Pt–Ru, it is likely to associate the $8e^-$ process to indirect oxidation, that is, Ru mainly serves as the BH_4^- hydrolysis catalyst to convert BH_4^- to adsorbed hydrogen, which migrated to Pt sites and was oxidized to water. Pt primarily acts as the electrocatalyst for adsorbed hydrogen oxidation [7].

3.2. Electrode characterization and fuel cell test

Morphologies of Ni foam, Pt–Ru/Ni foam electrode, Pt–Ru and Pd–Ir catalysts are shown in Fig. 2. The electrode has a three-dimensional network structure with open cages. Electrocatalysts form an intergrown layer on the surface of the skeleton of nickel foam. The width of the skeleton is about 100 μm (Fig. 2d). Pt–Ru and Pd–Ir present as clusters with a wide size distribution. Pt–Ru clusters are less agglomerated and smaller in size than Pd–Ir. EDX analysis indicates that the atomic ratio of Pt:Ru and Pd:Ir is 68:32 and 82:18, respectively.

Fig. 3 shows the performance of a DBHPFC with different concentrations of $NaBH_4$. The open circuit voltage is about 1.0 V, which is approximately 1.1 V lower than the theoretical value of an alkaline DBHPFC (2.11 V) [2]. Similar results have been reported by Choudhury et al. [19]. By using AB_5 and AB_2 alloys as anode cat-

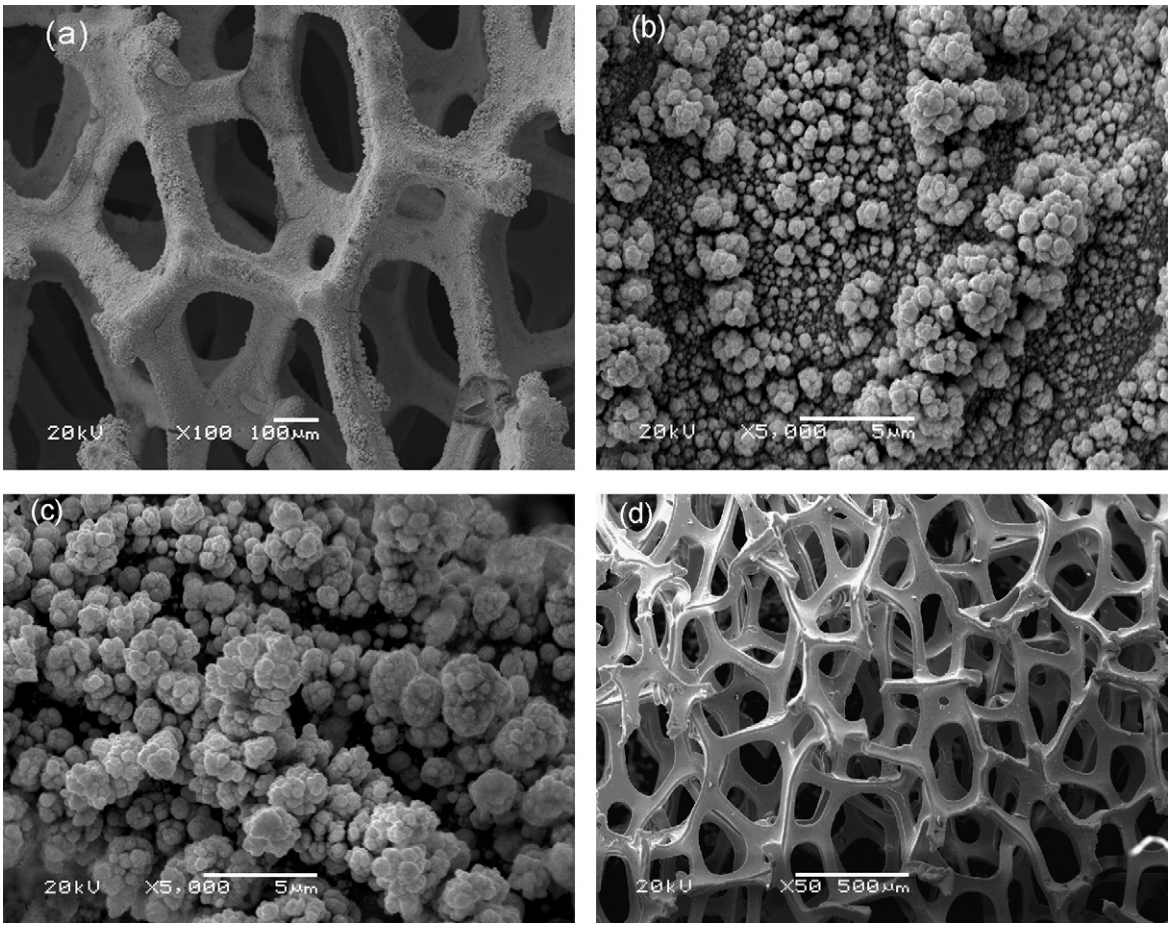

Fig. 2. SEM images of Pt–Ru coated nickel foam electrode (a), Pt–Ru anode catalyst (b), Pd–Ir cathode catalyst (c) and nickel foam (d).

alyst and Pt/C as cathode catalysts, they demonstrated an open circuit voltage of about 1.2 V. Such a large deviation of the open circuit cell voltage from the equilibrium cell voltage is likely due to the cathode polarization. Even though the standard potential for H_2O_2 electroreduction is 0.87 V vs. SHE, we consistently found that at various electrocatalysts, such as Au, Pt, Co_3O_4, the open circuit potential for H_2O_2 electroreduction in high concentration NaOH (e.g. 3 mol dm^{-3}) is about 0 V vs. SHE at room temperature. Bockris and Oldfield [20] reported that for H_2O_2 electroreduction in alkaline medium, the equilibrium potential of 0.87 V vs. SHE hold only at H_2O_2 concentration lower than 10^{-6} mol dm^{-3}, at higher H_2O_2 concentration, the equilibrium potential is essentially dependent only on pH value and the electrode material and is around 0 V vs. SHE in strong alkaline medium at Au and Pt electrode. The 0 V vs. SHE open circuit potential for H_2O_2 electroreduction at the cathode combines with an equilibrium potential of −1.24 V vs. SHE for BH_4^- oxidation at the anode give the alkaline DBHPFC an equilibrium voltage of around 1.22 V instead of 2.11 V. The cell voltage decays linearly with the increase of current density indicating a strong dependence of cell performance on the ohmic resistance (mainly ohmic polarization). This is likely due to the reticulated structure of the electrode. The thickness of the electrode is 1 mm, which is much larger than the thickness of catalyst layer (less than tens micrometer) of conventional MEA [21]. The mass transport control region is not observed even when current densities reach around 750 mA cm^{-2} demonstrating the excellent mass transport performance of the electrodes. The cell performance is nearly independent of BH_4^- concentration when it is higher than 0.2 mol dm^{-3}, and high power output is achieved at 0.1 mol dm^{-3} BH_4^-. The DBHPFC exhibits a maximum power density of 198 mW cm^{-2} at a current density of 397 mA cm^{-2} and a cell voltage of 0.5 V when operating on 0.2 mol dm^{-3} $NaBH_4$ at room temperature. No apparent hydrogen evolution was observed at borohydride concentration lower than 0.2 mol dm^{-3}. The rate of hydrogen generation on Ru due to hydrolytic decomposition of BH_4^- is slower at lower BH_4^- concentration. When the rate of hydrogen generation on Ru is slower than the rate of hydrogen oxidation on Pt, hydrogen generated on Ru will be completely consumed on Pt before releasing to the solution.

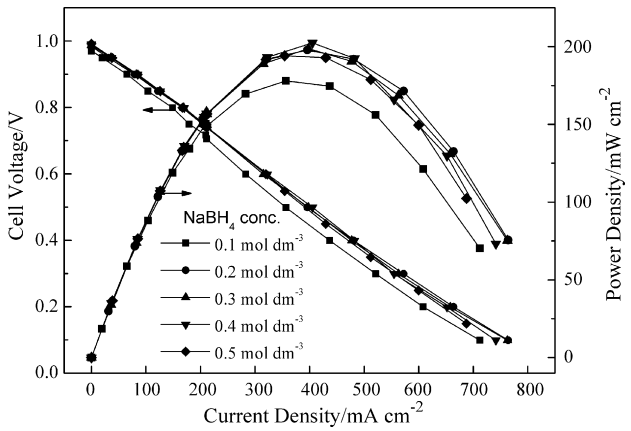

Fig. 3. Effects of borohydride concentration on the cell performance. Anolyte: x mol dm^{-3} $NaBH_4$ in 3 mol dm^{-3} NaOH (x = 0.1, 0.2, 0.3, 0.4 and 0.5). Catholyte: 0.4 mol dm^{-3} H_2O_2 in 3 mol dm^{-3} NaOH. Flow rate: 40 cm^3 min^{-1}. Room temperature.

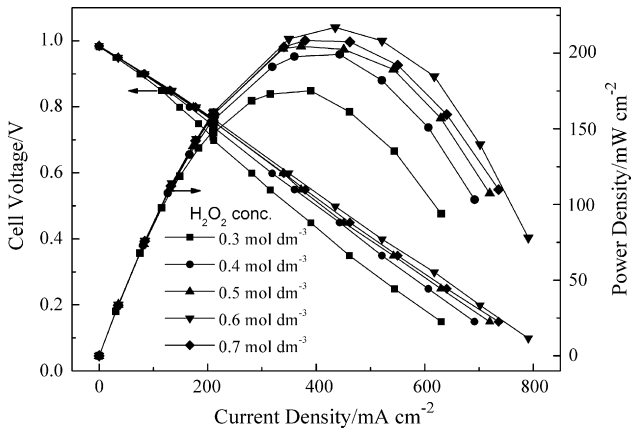

Fig. 4. Effects of hydrogen peroxide concentration on the cell performance. Anolyte: 0.2 mol dm^{-3} $NaBH_4$ in 3 mol dm^{-3} NaOH. Catholyte: x mol dm^{-3} H_2O_2 in 3 mol dm^{-3} NaOH (x = 0.3, 0.4, 0.5, 0.6 and 0.7). Flow rate: 40 cm^3 min^{-1}. Room temperature.

Fig. 4 shows the influence of H_2O_2 concentration on cell performance. The cell voltage–current density polarization curves have similar features as those in Fig. 3, i.e. nearly linear and no limiting current control region. The cell performance is improved with increasing H_2O_2 concentration from 0.3 to 0.6 mol dm^{-3}. However, further increase in H_2O_2 concentration up to 0.7 mol dm^{-3} causes a decrease in cell performance. This behavior is probably due to the decomposition of hydrogen peroxide, which produces gas bubbles that attach on electrode surface and reduce the effective electrode surface area. The decomposition of H_2O_2 become obvious when H_2O_2 concentration increased to 0.4 mol dm^{-3} and it is more significant at higher concentrations. The peak power density reaches 217 mW cm^{-2} at 435 mA cm^{-2} and 0.5 V running on 0.6 mol dm^{-3} H_2O_2 at room temperature.

Fig. 5 demonstrates the dependence of cell performance on the operation temperatures. Obviously, the cell performance improves with the increases of temperature up to 55 °C, but a further increase in temperature reduces the cell performance significantly. This reduction in cell performance is caused by the severe decomposition of $NaBH_4$ at the anode and H_2O_2 at the cathode. A lot of bubbles are observed at temperatures higher than 45 °C. The increase of operation temperature increases kinetics of both anode and cathode reactions, leading to the enhancement in power density of the fuel cell, however, it also speeds up the decomposition of $NaBH_4$ and H_2O_2, which result in the decrease of utilization efficiencies of $NaBH_4$ and H_2O_2. The cell can deliver a maximum power density of about 345 mW cm^{-2} at 630 mA cm^{-2} and 0.55 V at 55 °C, but at the expense of waste of the fuel and the oxidant. Therefore, for this type of fuel cell, operating at low temperature on low concentration fuel and oxidant is critical for minimizing gas evolution and achieving high reactants utilization efficiency. Choudhury et al. [19] recently reported an alkaline DBHPFC with a $M_mNi_{3.55}Al_{0.3}Mn_{0.4}Co_{0.75}$ (5 mg cm^{-2}) anode and a 60 wt.% Pt/C (1 mg cm^{-2} of Pt) cathode. The cell exhibited a peak power density of ca. 150 mW cm^{-2} at a cell voltage of 540 mV, which was obtained at operation temperature of 70 °C using 10 wt.% $NaBH_4$ as the fuel and 8.9 mol dm^{-3} H_2O_2 as the oxidant. Our cell reaches the similar performance but at significant lower operation temperature (25 °C) and low concentration of $NaBH_4$ (0.2 mol dm^{-3}) and H_2O_2 (0.4 mol dm^{-3}).

Fig. 6 shows the cell voltage–operation time curves measured at a constant discharge current density of 250 mA cm^{-2} and room temperature. This stability test is carried out in two operation modes. In the first hour operation, fresh anolyte (0.2 mol dm^{-3} $NaBH_4$ in 3 mol dm^{-3} NaOH) and catholyte (0.4 mol dm^{-3} H_2O_2 in 3 mol dm^{-3} NaOH) continuously flow through the cell from their individual reservoirs to their waste containers. So the concentrations of fuel, oxidant and electrolyte at the inlet of the fuel cell remain the same during the test period. The reaction products are flushed out of the cell, and therefore have less opportunity to accumulate inside the cell. Under this operation condition, the fuel cell displayed superior stability. The cell voltage decreased by about 20 mV in 1 h operation. After the first hour operation, the anolyte (150 cm^3) and the catholyte (150 cm^3) start to be circulated between their reservoirs and the fuel cell. In this operation mode, the cell voltage decreases almost linearly with the increase of time from 60 to 120 min, and decreases faster after this. The cell voltage drops by about 80 mV after the first hour operation and by about 250 mV in the total 2 h operation in the circulation mode. The decline of the cell voltage along with time in the circulation mode is likely due to an increase in the ohmic loss and decreases in the concentration of reactants. The increase in the ohmic loss might result from the increase of resistance to ionic transport through the membrane or through the electrolyte. The membrane could have been partially blocked by the products generated from the oxidation of $NaBH_4$ [2]. The crossover of $NaBH_4$ to the cathode and H_2O_2 to the anode might also have negative effects on the cell performance, primarily via the consumption of reactants because $NaBH_4$ and H_2O_2 react rapidly once in contact.

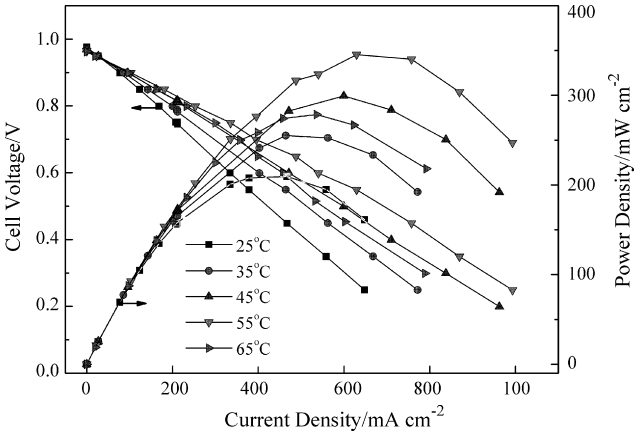

Fig. 5. Effects of operating temperature on the cell performance. Anolyte: 0.2 mol dm^{-3} $NaBH_4$ in 3 mol dm^{-3} NaOH. Catholyte: 0.4 mol dm^{-3} H_2O_2 in 3 mol dm^{-3} NaOH. Flow rate: 40 cm^3 min^{-1}.

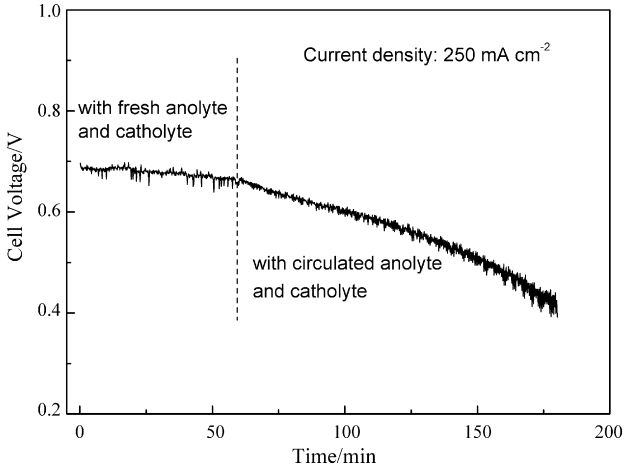

Fig. 6. Cell voltage–time curve recorded at a current density of 250 mA cm^{-2}. Anolyte: 0.2 mol dm^{-3} $NaBH_4$ in 3 mol dm^{-3} NaOH. Catholyte: 0.4 mol dm^{-3} H_2O_2 in 3 mol dm^{-3} NaOH. Flow rate: 40 cm^3 min^{-1}. Room temperature.

4. Conclusions

An liquid–liquid alkaline DBHPFC with high power density is demonstrated. The cell uses electrodes having three-dimensional network structure with open pores and operates at a low concentration of $NaBH_4$ and H_2O_2 at room temperature, which minimizes the evolution of H_2 at the anode and O_2 at the cathode. The high performance results from the unique electrode structure and the high activity of electrocatalysts. The cell exhibited an open circuit voltage of about 1.0 V and a peak power density of 198 mW cm^{-2} at of 397 mA cm^{-2} and 0.5 V using 0.2 mol dm^{-3} $NaBH_4$ as fuel and 0.4 mol dm^{-3} H_2O_2 as oxidant at room temperature. Complete $8e^-$ oxidation of $NaBH_4$ was observed on Pt–Ru nanoparticles in 2 mol dm^{-3} NaOH solution containing 0.01 mol dm^{-3} $NaBH_4$.

Acknowledgements

We gratefully acknowledge the financial support of this research by Heilongjiang Provincial Natural Science Foundation (ZJG2007-06-02), Heilongjiang Postdoc Foundation (LBH-Q06091), Harbin Science and Technology Fund for Young Scholars (2007RFQXG023) and Harbin Engineering University (HEUFT07030).

References

[1] R.K. Raman, N.A. Choudhury, A.K. Shukla, Electrochem. Solid State Lett. 7 (2004) A488–A491.
[2] C.P. de Leon, F.C. Walsh, A. Rose, J.B. Lakeman, D.J. Browning, R.W. Reeve, J. Power Sources 164 (2007) 441–448.
[3] G.H. Miley, N. Luo, J. Mather, R. Burton, G. Hawkins, L. Gu, E. Byrd, R. Gimlin, P.J. Shrestha, G. Benavides, J. Laystrom, D. Carroll, J. Power Sources 165 (2007) 509–516.
[4] C. Ponce de Leon, F.C. Walsh, C.J. Patrissi, M.G. Medeiros, R.R. Bessette, R.W. Reeve, J.B. Lakeman, A. Rose, D. Browning, Electrochem. Commun. 10 (2008) 1610–1613.
[5] L. Gu, N. Luo, G.H. Miley, J. Power Sources 173 (2007) 77–85.
[6] G. Selvarani, S.K. Prashant, A.K. Sahu, P. Sridhar, S. Pitchumani, A.K. Shukla, J. Power Sources 178 (2008) 86–91.
[7] V.W.S. Lam, E.L. Gyenge, J. Electrochem. Soc. 155 (2008) B1155–B1160.
[8] E. Gyenge, M. Atwan, D. Northwood, J. Electrochem. Soc. 153 (2006) A150–A158.
[9] H. Dong, R. Feng, X. Ai, Y. Cao, H. Yang, C. Cha, J. Phys. Chem. B 109 (2005) 10896–10901.
[10] B.H. Liu, Z.P. Li, S. Suda, Electrochim. Acta 49 (2004) 3097–3105.
[11] Z.P. Li, B.H. Liu, J.K. Zhu, S. Suda, J. Power Sources 163 (2006) 555–559.
[12] F.A. Coowar, G. Vitins, G.O. Mepsted, S.C. Waring, J.A. Horsfall, J. Power Sources 175 (2008) 317–324.
[13] C. Ponce-de-Leon, D.V. Bavykin, F.C. Walsh, Electrochem. Commun. 8 (2006) 1655–1660.
[14] M.H. Atwan, C.L.B. Macdonald, D.O. Northwood, E.L. Gyenge, J. Power Sources 158 (2006) 36–44.
[15] M. Chatenet, F. Micoud, I. Roche, E. Chainet, Electrochim. Acta 51 (2006) 5459–5467.
[16] D. Cao, J. Chao, L. Sun, G. Wang, J. Power Sources 179 (2008) 87–91.
[17] H. Cheng, K. Scott, Electrochim. Acta 51 (2006) 3429–3433.
[18] K.T. Park, U.H. Jung, S.U. Jeong, S.H. Kim, J. Power Sources 162 (2006) 192–197.
[19] N.A. Choudhury, R.K. Raman, S. Sampath, A.K. Shukla, J. Power Sources 143 (2005) 1–8.
[20] J.O. Bockris, L.F. Oldfield, Trans. Faraday Soc. 51 (1954) 249–259.
[21] H. Inoue, H. Daiguji, E. Hihara, JSME Int. J. Ser. B 47 (2004) 228–234.